Progress in Organic Coatings 180 (2023) 107552

Contents lists available at ScienceDirect

Progress in Organic Coatings

journal homepage: www.elsevier.com/locate/porgcoat

Reversible imine crosslinking in waterborne self-healing polymer coatings

Tiago D. Martins [a], M. Teresa Viciosa [a], Mariana B. Oliveira [b], Auguste Fernandes [a], João F. Mano [b], Carlos Baleizão [a,*], José Paulo S. Farinha [a,*]

[a] Centro de Química Estrutural, Institute of Molecular Sciences, Department of Chemical Engineering, Instituto Superior Técnico, Universidade de Lisboa, Av. Rovisco Pais, 1049-001 Lisboa, Portugal

[b] CICECO – Aveiro Institute of Materials, Department of Chemistry, University of Aveiro, 3810-193 Aveiro, Portugal

ARTICLE INFO

Keywords:
Polymer nanoparticles
Waterborne polymer coatings
Self-healing
Dynamic covalent bonds
Imine bond formation

ABSTRACT

Waterborne polymer coatings have the potential to address the environmental concerns associated with solvent based systems. To improve their performance without using volatile organic compounds, we propose a new approach based on reconfigurable covalent crosslinking that provides mechanical resistance and self-healing properties. The new waterborne polymer coatings are based on mixtures of aldehyde- and amine-functionalized polymer nanoparticles (PNPs) that take advantage of the reversibility of imine bonds in the presence of water. Different degrees of functional monomer incorporation (10 % to 40 %) allowed us to balance crosslinking and interdiffusion during film formation, to obtain mechanically robust and solvent resistant films. A clear structure-properties relation was assessed by following the formation of water resulting from amine-aldehyde condensation crosslinking, measured by differential scanning calorimetry. The resulting polymer coatings further show self-healing properties at room temperature, triggered with residual amounts of water and featuring high recovery rates of the mechanical properties. Our mechanically robust waterborne polymer coatings based in imine reversible crosslinking, featuring self-healing in mild conditions, offer excellent prospects for application in smart coating materials.

1. Introduction

Polymer dispersions produced by emulsion polymerization have wide application in waterborne adhesives, paints, and coatings, with increasing interest as a strategy with lower environmental impact and higher sustainability [1–3]. Traditional waterborne polymer coatings use volatile organic compounds (VOCs) to facilitate polymer interdiffusion below the glass transition temperature (T_g) of the polymer during film formation, to produce stronger films upon evaporation. With the need to reduce the use of VOCs by the coatings industry, it is still difficult for waterborne coatings based on dispersions of polymer nanoparticles (PNPs) to reach the high performance of their solventborne counterparts [4–6].

Waterborne polymer coatings are formed in three steps: evaporation of the solvent (water), deformation of the PNPs, and their coalescence by interdiffusion of the polymer chains [7]. Upon drying, the aqueous dispersion of PNPs originates a densely close-packed arrangement of the PNPs. This is followed by particle deformation to yield closer contact between particles, if the film is above the minimum film formation temperature (T_{mff}), which corresponds approximately to the T_g of the polymer in the presence of water. At this stage, the films still have weak interfaces between the PNPs. These are strengthened by polymer chain interdiffusion between adjacent PNPs, occurring for temperatures above the T_g of the polymer, leading to complete healing of the interfaces to form a mechanically rigid film [8–10]. The degree of entanglements between the polymer chains determines how strong the interface is [11].

Relying only in chain interdiffusion, while avoiding the use of VOCs, strongly limits the versatility and performance of the resulting films. Low T_g polymers have faster interdiffusion, better interface healing, but produce tacky films with low mechanical resistance. Higher T_g polymers could enhance mechanical properties, but their diffusion is slower and therefore interdiffusion between PNPs very limited. One strategy to overcome these limitations is to use polymer chains that have fast diffusion and are able to crosslink upon interdiffusion across the PNP interfaces [12,13]. By carefully balancing chain diffusion and crosslinking during film formation, the chains become anchored across the PNP interfaces (Fig. 1), increasing the mechanical resistance of the film. This balance between diffusion and crosslinking kinetics has been

* Corresponding authors.
E-mail addresses: carlos.baleizao@tecnico.ulisboa.pt (C. Baleizão), farinha@tecnico.ulisboa.pt (J.P.S. Farinha).

https://doi.org/10.1016/j.porgcoat.2023.107552
Received 17 July 2022; Received in revised form 23 February 2023; Accepted 18 March 2023
Available online 7 April 2023

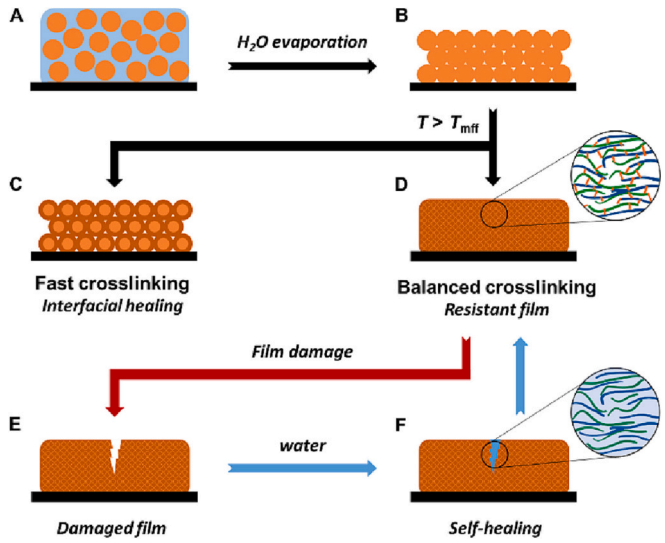

Fig. 1. Film formation in waterborne polymer dispersions: the balance of polymer chain diffusion between PNPs and crosslinking kinetics strongly impacts the final film properties and its self-healing ability in the presence of water. The PNP dispersion is casted onto the surface (A), and water evaporation leads to PNP packing (B). Fast crosslinking kinetics compared to polymer interdiffusion leads to interfacial crosslinking and weak films (C), while crosslinking after enough interdiffusion produces strong films (D). After damage of the film structure (E), exposure to water can revert crosslinking, allowing diffusion of the polymer chains, recovering of the film structure, and new crosslinking upon drying.

theoretically modelled by De Gennes et al. [14], who predicted that the mobility of the chains is reduced by fast crosslinking kinetics, which inhibits the healing of the interfaces and results in poor mechanical properties. However, if the crosslinking kinetics is slow enough to allow significant diffusion of the polymer chains across the PNP interfaces, locking of the system occurs only after significant interdiffusion and the films can develop good mechanical properties. Very slow crosslinking kinetics would increase curing times unnecessarily, with no advantage to the final mechanical properties.

Coating materials are continuously exposed to environmental agents, wearing down the material and leading to degradation and mechanical damage. Although conventional polyacrylate based waterborne coatings present good resistance to photodegradation and hydrolysis [15], these polymer networks cannot be reshaped once formed, which results in a limited lifetime [16]. The introduction of dynamic covalent bonds allows remodeling of the network upon exposure to an external stimuli such as heat, a catalyst or light. This strategy relies on manipulating the equilibrium of reversible reactions, so that, under specific external stimuli, the film crosslinks can be reconfigured [17,18]. Synthetic self-healing materials are a class of new emerging smart materials with the ability to heal small mechanical damages autonomously, opening a range of promising applications. Covalent self-healing can be based on Dies-Alder reactions, radical exchange, dynamic urea bond, transesterification, etc. [19] The reversibility of such reactions usually depends on external stimuli such as pH [20], light [21,22], temperature [23], pressure, or oxygen [24]. For example, Wouters et al. developed a coating using poly(butyl methacrylate) (PBMA) containing furfuryl methacrylate (FMA), where the low glass transition temperature of PBMA provided high chain mobility at low temperatures [25], facilitating network rearrangement by reversible Diels-Alder reaction [26]. Films of crosslinked PBMA, prepared from different functionalized PNPs, can exhibit substantial toughness and elongation at break at room temperature [27,28]. Another type of reversible crosslinking is based on the reaction between carbonyl and amine groups. For instance, systems based on keto-dihydrazide crosslinking show fast reaction rates at room temperature, which are reversible upon water addition [29]. However, this type of crosslinking resulted in only small improvements of the mechanical properties of the film due to poor kinetics, and use toxic components [30,31].

Imine bonds are also reversible in the presence of water, offering a very promising approach for dynamic covalent systems. Imine crosslinking encompasses two distinct processes: imine formation/hydrolysis, and imine exchange [32]. Imine bonds resulting from the condensation between amino and carbonyl groups (releasing a water molecule), can undergo rapid degenerative bond exchange without any significant side reactions [33]. The addition of water leads to the hydrolysis of the imine, with recovery of the starting groups [34,35]. Imine reversibility can thus be triggered by the presence of water [36], offering promising opportunities for use in polymer systems. When used for polymer crosslinking, imine bonds would therefore allow defect correction and reshaping of the polymer network in the presence of water. This offers an environmentally friendly, economical, and efficient polymer network reshaping method, for self-healing applications requiring only water as the external stimulus [32,37].

Despite the vast diversity of aldehyde and primary amine-containing monomers available, there are only a few studies on imine crosslinking in polymer networks [32,33,38]. These examples are solvent borne polymer networks, composed of only imine crosslinking monomers, and resulted in robust and highly recyclable films. These studies show that imine bond exchange is catalyzed by the presence of primary amines, and that the rate of exchange is dependent on the solvent, temperature, and imine structure.

Here we present a new waterborne polymer coating system that uses imine reversible covalent crosslinking to achieve good mechanical properties and solvent resistance, as well as self-healing properties in very mild conditions (room temperature and the presence of a small amount of water). The dispersion is a mixture of PNPs polymerized from butyl methacrylate (BMA), butyl acrylate (BA), and either an aldehyde or an amine functionalized methacrylate. Our environmentally friendly waterborne coating can form films at low temperatures, combining good flexural properties and mechanical strength due to the balance between diffusion and crosslinking, and show good self-healing properties in the presence of trace amounts of water.

2. Results

Functional polymer coatings were obtained from aqueous dispersions containing mixtures of polymer nanoparticles (PNPs) polymerized from butyl methacrylate (BMA), butyl acrylate (BA), and either aldehyde or amine functionalized methacrylates (PNP-CHO and PNP-NH2, respectively, Scheme S1). Upon casting and drying the dispersions, diffusion of polymer chains across the interparticle boundaries led to the formation of reversible imine bonds between the chains.

In the following sections we show the effect of this crosslinking in the mixed films, regarding their solvent resistance, mechanic performance and self-healing properties.

2.1. Synthesis of the polymer nanoparticles

PNPs were obtained by a modified semi-batch emulsion polymerization procedure [39], so that the composition of the formed copolymer is the same as the monomer mixture in the feed. A non-charged hydrophobic initiator (AIBN) was chosen to prevent polymerization of the water soluble funcrional monomers in the aqueous phase [40]. The AIBN initiator was mixed in the monomers phase before feeding to the reactor. The amine monomer used in the preparation of PNP-NH2, *N*-(3-aminopropyl)methacrylamide hydrochloride (APMA), resists the polymerization and testing conditions, contrarily to the similar *N*-(2-aminoethyl)methacrylate hydrochloride, which was shown to be pH-susceptible to acyl migration [40,41], with the nucleophilic intramolecular attack of the amine on the carbonyl group resulting in a more

stable molecule but without a primary amine. In separate batches, aldehyde and amine functionalized nanoparticles (PNP-CHO and PNP-NH2) were synthesized with different amounts of the functional monomers (10, 20, 30 and 40 %).

The hydrodynamic diameter of the different PNPs, measure by DLS (Table 1 and Fig. 2), range from 50 nm and 500 nm, but with a low size dispersity in all cases. The different diameters obtained reflect the effect of reacting conditions and monomers on PNP nucleation, and therefore on PNP diameter [42,43].

For PNP-CHO samples, the addition of a surfactant (CTAB) stabilizes the particle formation. For increasing amounts of MA, the particle diameter is smaller probably due to lower steric hindrance of MA compared to BMA, which allows a better packing of the polymeric chains, resulting in smaller PNPs (Fig. 2A). On the other hand, for PNPs-NH2, larger contents of functional monomer APMA resulted in larger particles (Fig. 2B). This is probably due to the increase in amine groups relative to the acrylate carbonyl groups leading to particle swelling (increase in hydrogen bonds between the polymer and water), increasing the viscosity of the mixture. This is in agreement with the study presented by Grabs et al. [40], reporting an increase in PNP size upon increasing the content of the amine monomer (2-aminoethyl methacrylate hydrochloride) in a copolymerization with BMA.

The polymerization reaction was followed by ^{1}H NMR using trioxane as internal standard to quantify the monomer conversion. In general, the conversion is high for all monomers, showing conversion rates above 98 % for PNP-0, and above 94 % for PNP-CHO (Fig. S1). For PNP-NH2 the conversion rates varied between 75 % and 90 % (corresponding to a minimum of APMA that stay in the aqueous phase due to its relatively high water solubility, Fig. S2) [40].

2.2. Film formation

Different dispersions were cast onto Teflon substrates, dried at 40 °C for 48 h, and then annealed at 80 °C for 1 h. The BMA/BA monomer ratio was chosen to have a glass transition temperature (T_g) below room temperature. This yields good chain mobility at relatively low temperature, leading to the formation of transparent films under ambient conditions (Fig. S3).

Films cast from non-functionalized PNPs, polymerized from only BMA and BA (PNP-0), PNPs with 20 % CHO (PNP-20%CHO), 20 % NH_2 (PNP-20%NH2) and from a mixture of PNP-20%CHO and PNP-20%NH2 (PNP-20%MIX), were characterized by ATR-FTIR (Fig. 3). The film cast from PNP-0 shows only characteristic vibrations at 2975–2877 cm^{-1} (weak) for the aliphatic C—H bonds, 1726 cm^{-1} (medium) for the C═O bonds and at 1463 cm^{-1} (weak) for the C—C bonds, which are present in all samples. The films cast from aldehyde containing polymer (PNP-20% CHO) resulted in very similar spectra because the carbonyl groups signal of the acrylates and the aldehyde are found at the same wavenumber (1726 cm^{-1}). A different peak appears at 2861 cm^{-1} (weak), attributed to the asymmetric stretching of the O=C-H of the aldehyde group [38,42]. The films cast form amine functionalized nanoparticles (PNP-20%NH2) show the characteristic vibrations of amine groups at 3324 cm^{-1} (stretch, weak) and 1533 cm^{-1} (weak). This sample also shows a vibration at 1623 cm^{-1} (bend, weak) which is attributed to the bending of the H-N-C=O [44,45].

The films cast from mixtures of amine and aldehyde functionalized PNPs (PNP-20%MIX) resulted in a combination of all the peaks described above. Nonetheless, a small shoulder at 1645 cm^{-1} (weak) shows the formation of a new bond, consistent with the vibrations of imine bonds (N=C) [33], which corresponds to the crosslinking reaction between aldehyde and amine functionalized polymer chains from different PNPs. Similar spectra were obtained at different concentrations of functional groups (Fig. S4), showing successful imine crosslinking.

Table 1
Mean PNP hydrodynamic diameter obtained by DLS (nm).

Functional group (%)	PNP-CHO	PNP-NH2
10	127 ± 2	149 ± 5
20	92 ± 2	198 ± 3
30	70 ± 1	242 ± 7
40	56 ± 1	466 ± 11

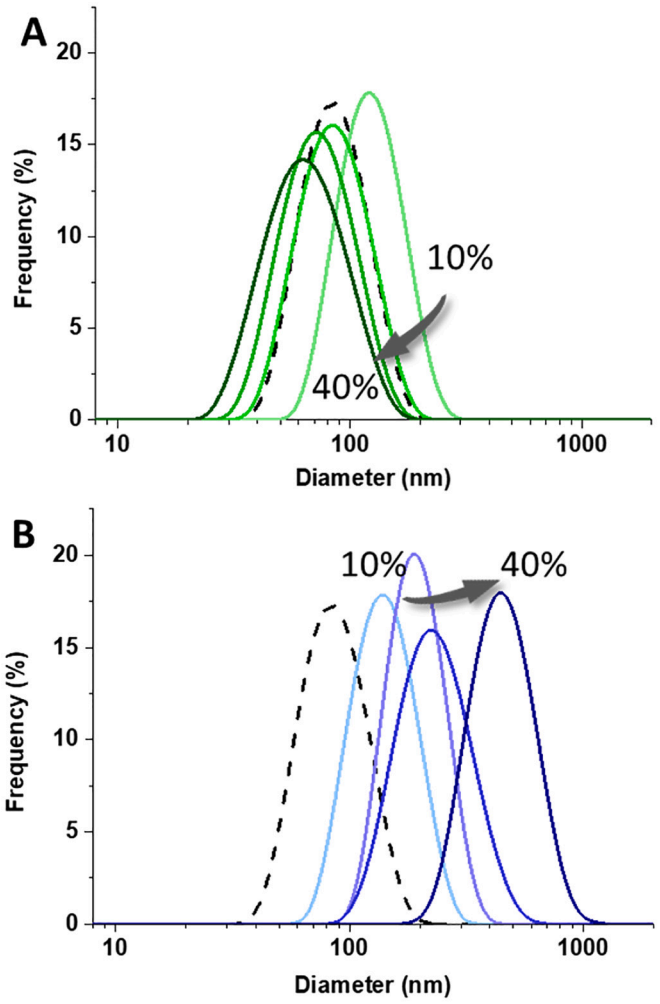

Fig. 2. Hydrodynamic diameter distribution (obtained by DLS) for: PNP-0 polymerized from only PBMA and BMA (dashed black lines), aldehyde-functionalized PNP-CHO (A, green lines) and amine-functionalized PNP-NH2 (B, blue lines). The darker lines (and arrows) indicate increasing fraction of functional groups (10 % to 40 %). (For interpretation of the references to colour in this figure legend, the reader is referred to the web version of this article.)

2.3. Swelling tests and solvent resistance

The interaction of the polymer films with good solvents for the polymer is a clear and simple way of evaluating the degree of cross-linking in the film [27,46]. Also, solvent-resistance widens the possible applications of the coating material. Solvent swelling of a non-crosslinked film promotes disentanglement of the polymer chains and ultimately destroys the network. Here we used THF, a good solvent for P (BMA-BA) as confirmed for film cast from PNP-0 (Table 2). The films were washed with THF, filtered with a 0.45 μm PTFE membrane and dried at 60 °C.

As expected, imine crosslinking in the film led to the formation of a polymer network with higher solvent resistance, measured by the remaining macroscopic gel (*RMG*) (Table 2). Higher *RMG* values were obtained for films cast from PNP-40%MIX (89 ± 5), with lower *RMG*

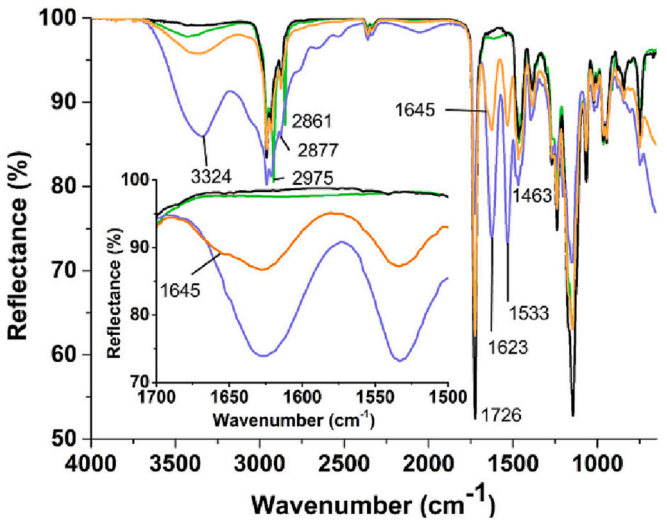

Fig. 3. ATR-FTIR of polymer films cast from PNP-0 (black line), PNPs-20%CHO (green line), PNP-20%NH_2 (blue line) and PNP-20%MIX (orange line). (For interpretation of the references to colour in this figure legend, the reader is referred to the web version of this article.)

Table 2
Swelling degree (*Q*), remaining macroscopic gel % (*RMG*), crosslinking density (*dX*), and average mass between crosslinkings (*Me*) of polymer films casted from PNP-0 and PNP-10%MIX to PNP-40%MIX and immersed in THF at room temperature.

Sample	*RMG* (wt%)	*Q* (%)	*dX* (mol.cm^{-3})	*Me* (g.mol^{-1})
PNP-0	0	–	–	–
PNP-10%MIX	64 ± 2	310	1.1×10^{-5}	5.0×10^{4}
PNP-20%MIX	32 ± 3	134	2.1×10^{-4}	2.5×10^{3}
PNP-30%MIX	58 ± 7	165	1.8×10^{-4}	2.9×10^{3}
PNP-40%MIX	89 ± 5	114	–	–

values obtained for functional group contents in-between: 58 ± 7 for PNP-30%MIX and only 32 ± 3 for PNP-20%MIX.

The amount of imine crosslinking in the films is measured by the crosslinking density (*dX*), which was estimated from the swelling degree (*Q*) – see Section 4.5 below for calculation details. Table 2 shows that the increase in functional groups content approximately results in lower *Q* values as expected, with the changes in *dX* (and in the average mass between crosslinkings, *Me*) mirroring those of *Q*. The values of *dX* and *Me* for PNP-40%MIX were not estimated due to the error associated with the very low *Q* value, and assuming that the density of the copolymer is equal to the density of PBMA.

The explanation for these results is related to the balance between the kinetics of polymer diffusion and imine formation. For low functional group content (10 %), the polymer chains diffuse further due to the low number of anchoring points, yielding a film with good solvent resistance (high *RMG*), despite the relatively low crosslinking density (low *dX* and high *Me*, resulting in a large *Q*).

With the functional groups content increasing to 20 %, imine formation hinders polymer diffusion, and a homogeneous distribution of crosslinks across the film is not achieved. Therefore, although *dX* increases (with a decrease in *Me* and lower *Q*), the resistance to solvent decreases (lower *RMG*). At higher functional groups content, even though interdiffusion is strongly hindered, the amount of crosslink points is enough to create a dense polymer network with high solvent resistance.

2.4. Mechanical properties and self-healing

Films cast from functionalized and non-functionalized PNPs were tested for the Young's modulus, tensile strength, elongation at break and toughness (Fig. S5). We also evaluated the self-healing of functionalized and non-functionalized polymer films, to assess the performance of the imine reversible crosslinking approach. To this end, the films were cut transversally, and the two pieces superimposed with addition of 5 μL of water to moisten the film (see Scheme S2). These films were then kept overnight at room temperature. The results of the mechanical tests shown in Fig. 4 reflect the balance between the kinetics of crosslinking and polymer interdiffusion across the PNP interfaces, with the interparticle crosslinking reaction restricting the interdiffusion of the polymer chains during film formation [11,47]. Higher content of functional groups leads to more crosslinking points that reduce the interdiffusion of the polymer chains, impairing the mechanical performance of the films as expected [48].

Among the non-damaged films (green points in Fig. 4), the films obtained from PNP-0 show relatively good mechanical properties, combining strength and elasticity, with a 4.5 ± 0.3 MPa tensile strength, 147 ± 12 MPa Young's modulus, 189 ± 8 % elongation at break, and 861 ± 94 MPa toughness. Similar results were obtained by Pinenq et al. [49] for uncrosslinked films of PBMA-BA. The film cast from PNP-10% MIX show a higher tensile strength (5.7 ± 1.2 MPa), but lower Young's modulus and toughness. Therefore, the presence of crosslink points did not compensate the decrease in chain interdiffusion. With an increase in functional groups density to 20 % (PNP-20%MIX), weaker films (lower tensile strength, modulus, and toughness) were obtained. Nonetheless, they showed higher elasticity, with an elongation at break of 277 ± 16 %. The further decrease in film resistance follows the decrease in chain interdiffusion due to crosslinking, while the increase in crosslink points compensates the decrease in chain entanglement and provides better network elastic response. Above 20 % of functional groups, the Young's modulus increases, probably due to the crosslinking density capable of compensating the decrease in polymer interdiffusion. However, the increased crosslink density yields more rigid films, with lower toughness and elongation at break.

The crosslinking efficiency explaining the mechanical behavior of the samples also correlate well with the solvent resistance results. For PNPs with 20 % functional groups, the fast superficial crosslinking between chains, prevents chain interdiffusion (Fig. 5) [50]. For higher functional group density (30 % and 40 %), the increase in crosslink density compensated the decrease in chain interdiffusion yielding better solvent resistance, although with no improvement in mechanical

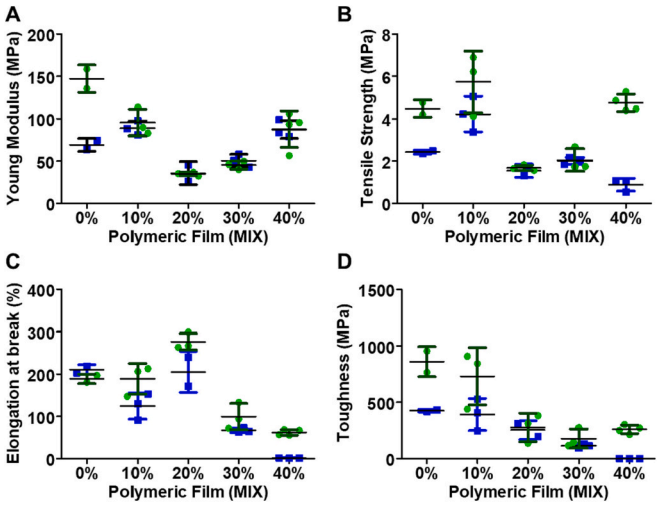

Fig. 4. Mechanical properties of the polymeric films, as cast (green dots) and after self-healing at room temperature (blue squares). A) Young's Modulus; B) Tensile Strength; C) Elongation at break; D) Toughness. (For interpretation of the references to colour in this figure legend, the reader is referred to the web version of this article.)

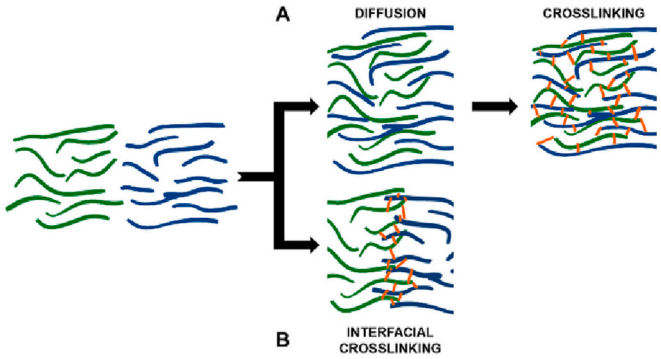

Fig. 5. Cartoon illustrating interdiffusion and crosslinking of polymer chains from two adjacent polymer nanoparticles during film formation: A) balanced diffusion/crosslinking leading to mechanically strong film; and B) fast interfacial crosslinking inhibiting chain interdiffusion.

properties.

The crosslinked films tested after breaking and self-healing at room temperature in the presence of water show very good recovery of the mechanical properties (blue points in Fig. 4), except to PNP-40%MIX and the uncrosslinked PNP-0 films. To compare the self-healing capacity of the different films, we calculate the recovery (%) of their mechanical properties relative to the initial (undamaged) films (Fig. 6). The non-functionalized healed films cast from PNP-0 could achieved only ~50 % of their initial modulus, tensile strength and toughness (although with a good recovery of the elongation). This is probably because for these films, healing happens only due to interdiffusion, which is limited at room temperature in spite of the low T_g.

On the other hand, the films prepared from mixtures of functional PNPs generally show a significative recovery of the mechanical properties after self-healing, due to the reversible imine crosslinking. All the healed functional films present a full recovery of their modulus, and most show relatively good recovery of the other properties, except the film of PNP-40%MIX. Similar recovery rates were obtained by Chakma et al. [51] on a solvent-borne 2-hydroxyethyl acrylate polymer matrix with a thiol-maleimide crosslinking. However, not only this formulation was solvent-borne and had lower mechanical strength (on the kPa range), but the high recovery rates could only be achieved at high temperature and/or pH values.

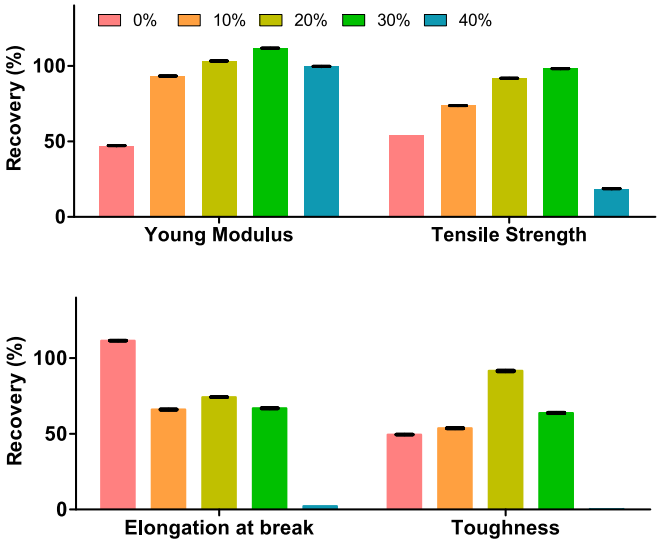

Fig. 6. Recovery rate of the film mechanical properties after self-healing at room temperature in the presence of water: Young's modulus; tensile strength; elongation at break; and toughness.

In general, the functional films prepared from PNP-10%MIX, PNP-20%MIX and PNP-30%MIX offer excellent perspectives for the development of advanced self-healing coatings, requiring only water as external stimuli for recovery [32,36,38].

The self-healing performance of the functional films can be explained by the reversibility of the imine formation reaction. The presence of a low amount of water can affect the imine bonds of the wetted area, leading to reconfiguration of the crosslinking points by imine hydrolysis and formation, transamination or imine metathesis (Fig. 7) [38].

2.5. Differential scanning calorimetry

To characterize the thermal behavior of the PNPs, in particular the imine bond formation and the glass transitions, essential for film formation, different PNP dispersions (PNP-10%CHO, PNP-10%NH2 and PNP-MIX10% to PNP-MIX40%) were analyzed by Differential Scanning Calorimetry (DSC). For the sample PNP-10%CHO, the first thermogram obtained on cooling (Fig. 8) shows an exothermal peak (onset temperature, $T_{on} \approx -20$ °C), associated with the crystallization of water present in the dispersion. The corresponding melting peak is observed on the subsequent heating at T_{min} = 1.9 °C. On subsequent cycles, with increasing final temperatures (see Scheme S3 and Fig. S6), a different exothermal peak appears, which is visible with an onset around - 38 °C (green line in Fig. 8), whose intensity increases as the final temperature of the cycles increases. Although both exothermal peaks can be attributed to water crystallization, their different behavior must be noted: while the peak located close to - 20 °C is suppressed when the sample is heated to 100 °C, the peak at lower temperatures only disappears when the sample is heated to 120 °C.

One possible explanation for the presence of two water crystallization peaks is related to the location of the water molecules relative to the polymer chains. The aqueous media surrounding the PNPs must behave as bulk water whose crystallization occurs close to - 20 °C. However, as the T_{final} of the cycle reaches temperatures above the glass transition temperature, polymer chain diffusion becomes significative. Chain diffusion leads to an increase of the polymer in contact with water, allowing more water-polymer interactions. Such "new" interactions may originate a second type of water signal, whose crystallization is shifted to lower temperatures, as already reported in other systems including polymers [52]. This would explain the increase in the area of the lower temperature crystallization peak as T_{final} increases, reflecting the increase in the amount of water involved in the transition (at the same time that part of the water is being evaporated).

Regarding the glass transition of the sample, this can be only observed when most of the water has been removed (i.e., only when the sample is heated to 100 °C), whose midpoint is found at ca. 16.6 °C. The fact that no glass transition is observed in the presence of water is probably due to the overlap with the signals of water transformations (melting and/or evaporation), rather than a very pronounced plasticizing effect that would shift the T_g to values lower than - 80 °C.

The PNP-10%NH2 sample only shows one crystallization peak, whose onset is continuously shifted from - 20 to - 32 °C, as water is removed by the thermal treatment. This sample is more hydrophilic (due to hydrogen bonds), yielding a more homogeneous water distribution.

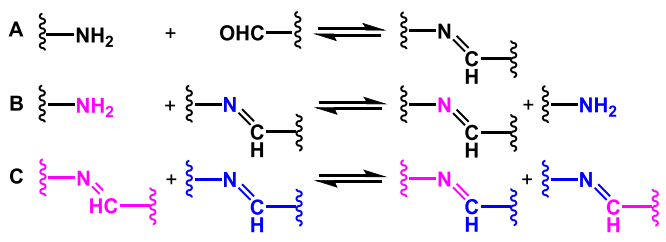

Fig. 7. Possible reactions during reconfiguration of the polymer network: A) imine hydrolysis and formation; B) transamination; C) imine metathesis.

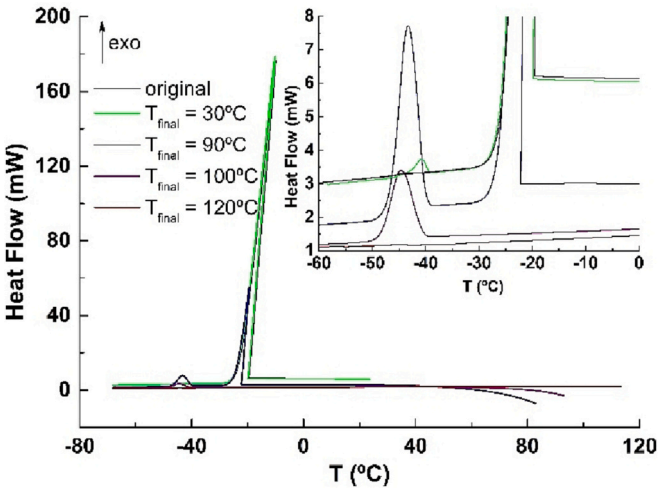

Fig. 8. Heat flow thermograms obtained upon cooling a water dispersion of PNP-10%CHO at a rate of 10 °C min^{-1} of (m_0 = 13.3 g, m_{end} = 6.1 g, ~54 wt% water), subjected to the thermal cycling treatment depicted in Scheme S3. The inset shows the lower temperature region featuring two distinct exothermal peaks associated with water recrystallization. See supporting information (Fig. S6) for the complete series of cooling thermograms.

Such shift in the onset of recrystallization may indicate that the water remaining after each thermal cycling is progressively closer to the polymer chains, and therefore slightly more difficult to undergo recrystallization. Once the sample reaches T_{final} = 90 °C, recrystallization of water is no longer detected. In this sample, the glass transition is detected in the initial state (Fig. 9 and S7), whose onset on heating is found at ca. - 48 °C (inset of Fig. 9). When most water is removed, the T_g is shifted to higher temperatures (Table 3), at ca. 18.6 °C (on cooling), which is probably related to a plasticizing effect of water.

The mixture of PNP-10%CHO and PNP-10%NH2 (PNP-10%MIX) shows the onset of "free" water recrystallization close to - 20 °C on cooling, with a small shift to lower temperatures as T_{final} increases (Fig. 10 and S8). Additionally, a second crystallization peak is observed after heating to 70 °C, with an onset below - 42 °C. The temperature, shape and intensity of the low-temperature peak, indicate an origin

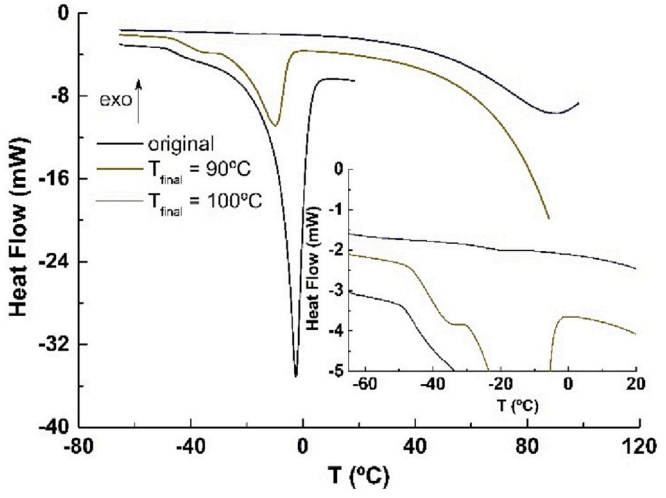

Fig. 9. Heat flow thermograms obtained upon heating a water dispersion of PNP-10%NH2 at a rate of 10 °C min^{-1} (m_0 = 12.9 g, m_{end} = 5.4 g, ~58 wt% water), subjected to the thermal cycling treatment depicted in Scheme S2. The inset enlarges the low temperature region evidencing the glass transition signal followed by the melting peak in the thermogram obtained before heating the sample at 90 °C. See supporting information (Fig. S7) for complete series of cooling thermograms.

Table 3
Glass transition temperatures determined on cooling the dried samples under modulated conditions (A = 0.218 °C, P = 60 s and cooling rate of 2 °C min^{-1}); the value of T_g was taken from the maximum of the derivative of the reverse component of the heat flow.

Sample	T_g (°C)
PNP-0	14.0
PNP-10%MIX	23.9
PNP-20%MIX	21.2
PNP-30%MIX	22.6
PNP-40%MIX	23.8

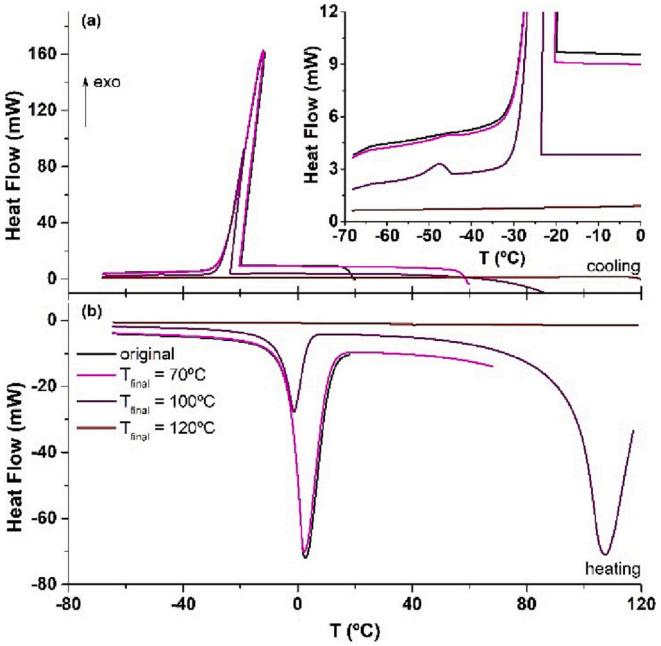

Fig. 10. Heat flow thermograms obtained at 10 °C min^{-1}: (a) on cooling and (b) on heating of PNP-10%MIX- a water dispersion of PNP-10%CHO and PNP-10%NH2 (m_0 = 19.3 g, m_{end} = 5.16 g, ~73 wt% water) - subjected to the thermal cycling treatment depicted in Scheme S4. The inset in (a) enlarges the low temperature region evidencing the second exothermal peak at temperatures around −45 °C. See supporting information (Fig. S8) for complete series of cooling thermograms.

different from that of the peak observed for isolated PNP-10%CHO (in PNP-10%NH2 no exothermal peaks were observed at lower temperature). A possible explanation for this difference is the composition of the PNP-10%MIX sample, for which the heating above 60 °C probably promotes the crosslinking reaction involving imine bond formation. This condensation reaction leads to the release of water, which is directly in contact with the polymer and probably behaves as confined water, with a recrystallization at lower temperatures [53]. When the sample is heated above 100 °C, no signal of recrystallization (either at −20 °C or - 45 °C) is detected, probably due to rapid evaporation of the water released upon imide formation.

For the PNP-30%MIX sample, a small but clear exothermal peak close to - 40 °C is detected after 30 min at 60 °C (Fig. S9). This can be attributed to the water produced by imine formation at that temperature. Relatively to the PNP-20%MIX sample, a change in the heat flow signal around - 40 °C indicates the presence of this "type" of water from the beginning. However, this changes only slightly as the sample is heated/dried, suggesting that the crosslinking reaction occurs to a lower extent at room temperature as expected.

The T_g values of the dried samples (Table) were determined from cooling thermograms measured between 100 and -70 °C, using temperature modulated differential scanning calorimetry (TMDSC) in order to better resolve the glass transition signal (details of the measurements in Section 5 in Supporting Information). The value of T_g for PNP-0 is ca. 10 °C lower that for the functional samples (PNP-10%MIX to PNP-40% MIX), but no difference was detected between these.

3. Conclusions

Emulsion polymerization was used to produce new functionalized PNPs for waterborne polymer coatings with reconfigurable crosslinking based on imine formation. The effect of the balance between crosslinking and interdiffusion was assessed by tensile and solvent-resistance tests, leading to a clear structure-properties relationship. We found that the introduction of only 10 % of functional groups can improve the solvent-resistance of the films by 65 %, while maintaining the mechanical performance of the material. In addition, the imine reversible crosslinking allowed self-healing of the films in very mild conditions, at room temperature and with a residual amount of water. The healed films presented very high recovery rates of the mechanical properties. Our novel waterborne smart polymer coatings open an excellent opportunity for developing VOC-free mechanically robust polymer coatings, featuring self-healing properties in simple and mild conditions. The system, featuring humidity-triggered crosslinking reversibility, allows the recovery from minor cuts and abrasion of the polymer film. Possible applications include coatings that are not in direct contact with water or high humidity environments (such as surgery rooms, clean rooms, electronic components etc.)

4. Experimental part

4.1. Materials

Butyl methacrylate (BMA, Aldrich, 99 %) and butyl acrylate (BA, Aldrich, 99 %) were used after passing through a column of aluminum oxide (Sigma-Aldrich, activated, basic, 58 Å pore size). Methacrolein (MA, Aldrich, 95 %), *N*-(3-aminopropyl)methacrylamide hydrochloride (APMA Aldrich, 98 %), hexadecyltrimethylammonium bromide (CTAB, Sigma, 99 %), 2,2-azobis(2-methylpropionitrile) (AIBN initiator, Alfa Aesar, 99.99 %) were used as received. Deionized water from a Millipore system Milli-Q ≥ 18 MU cm was used.

4.2. Synthesis of polymer nanoparticles (PNP)

All PNPs are polymerized from a mixture of BMA and BA. We produced PNPs without further functionalization (PNP-0), and PNPs that also incorporated either MA or APMA, to obtain aldehyde- and amine-functionalized PNPs, identified as PNP-CHO and PNP-NH2, respectively. In a sealed vial, 0.01 g (0.06 mmol) of AIBN was dissolved in 0.911 g (6.4 mmol) of BMA and 0.091 g (0.7 mmol) of BA and purged for 10 min. In another flask, 0.024 g (0.06 mmol) of CTAB was dissolved in 5 mL of water and purged for 10 min. Both solutions were slowly added to a Schlenk tube with 2.5 mL of water for 3.5 h. The mixture was stirred at 500 rpm at 65 °C for 5 h under argon atmosphere. The dispersion was then left to cool, filtered with glass wool, and stored at room temperature. For the aldehyde-functionalized nanoparticles (PNP-CHO), the MA was mixed with the other monomers. For the amine-functionalized nanoparticles (PNP-NH2), the APMA was dissolved in the aqueous phase and used as surfactant instead of the CTAB. Table 4 summarizes the composition of the monomer feed in each PNP synthesis. The amount of water and initiator was kept constant for all the synthesis.

4.3. Film formation

The PNP dispersions were cleaned with an ion exchange resin (Bio-Rad AG 501-X820-50) to remove surfactant and other water-soluble ionic materials. The dispersions were filtered with glass wool, casted on a Teflon substrate (5 × 3 cm) and dried at 40 °C for 48 h. The films were then annealed at 80 °C for 1 h. The film edges were removed so the final samples would have a uniform thickness. Each film was cut into 6 pieces (0.8 × 3 cm) for further mechanical performance evaluation.

Crosslinked films were obtained by mixing aldehyde- and amine-functionalized PNPs in a 1:1 M ratio (PNP-MIX) and were subjected to the same treatment as the non-functionalized PNPs.

Table 4
Monomer feed composition (mol%) of the different PNPs.

	BMA	BA	MA	APMAAH
PNP-0	90	10	–	–
PNP-10%CHO	81	9	10	–
PNP-10%NH2			–	10
PNP-20%CHO	72	8	20	–
PNP-20%NH2			–	20
PNP-30%CHO	63	7	30	–
PNP-30%NH2			–	30
PNP-40%CHO	54	6	40	–
PNP-40%NH2			–	40

4.4. Self-healing tests

Films of 0.8 × 3 cm were cut in half for self-healing evaluation. The films were wetted with 5 μL of H_2O on the overlaying edges and superimposed ca. 1 mm. A metal plate was used to fix the films and allow them to stay straight. Parchment paper was used to avoid adherence onto the substrate. The films were dried overnight at room temperature.

4.5. Swelling and solvent resistance evaluation

The swelling and solvent resistance of the films was tested by cutting small pieces of the previously formed films, which were weighted (m_1) and submerged under 3 mL of THF (a very good solvent for P(BMA-BA) for 24 h. The films were then washed with 200 mL of THF, filtered with a 0.45 μm poly(tetrafluoroethylene) (PTFE) membrane on a Millipore filtration kit, weighted (m_2) and dried to constant weight (m_3) at 60 °C.

The remaining macroscopic gel (RMG, wt%) corresponds to the ratio between the mass of the dried film (m_3) and the mass of the initial film (m_1) [46]. The swelling degree (Q) was estimated as [54]

$$Q = \left[1 + \rho_P\left(\frac{m_2}{m_1.\rho_{THF}} - \frac{1}{\rho_{THF}}\right)\right] \times 100\% \quad (1)$$

where ρ_P is the specific density of the polymer (considered equal to the density of PBMA, $\rho_P = 1.053$), and ρ_{THF} is the specific density of the solvent THF ($\rho_{THF} = 0.888$).

The apparent crosslinking density (dX) and the average mass between crosslinks (Me) were calculated as [55]

$$dX = \frac{ln(1-\phi_P) + \phi_P + \chi\,\phi_P{}^2}{2V_S\left(0.5\,\phi_P - \phi_P{}^{1/3}\right)} \quad (2)$$

$$Me = \frac{V_S.\rho_P\left(\phi_P{}^{1/3} - 0.5\,\phi_P\right)}{-\left[ln(1-\phi_P) + \phi_P + \chi\,\phi_P{}^2\right]} \quad (3)$$

where V_S is the molar volume of the solvent (81.2 $cm^3.mol^{-1}$ for THF at room temperature), ϕ_P is the volume fraction of the polymer in the swollen sample obtained from

$$\phi_P = \frac{m_3}{m_3 + (m_2 - m_3).\frac{\rho_P}{\rho_{THF}}} \quad (4)$$

and χ is the Floty-Huggins interaction parameter estimated as [56]

$$\chi = \frac{1}{2} + \frac{\phi_P}{3} \quad (5)$$

4.6. Methods

4.6.1. Dynamic Light Scattering (DLS)

PNP hydrodynamic diameters were measured by DLS using a Zetasizer Nano ZS (Malvern Instruments, UK). The PNP aqueous dispersions were diluted as required and measured at room temperature.

4.6.2. ^1H NMR

Solution ^{1}H NMR data were collected on a Bruker Avance III 400 spectrometer (Bruker BioSpin GmbH, Rheinstetten, Germany) operating at 400 MHz. Samples were prepared by dispersing 150 μL of functionalized PNPs in 350 μL of acetone-d_6. A known amount of 1,3,5-trioxane was added as internal standard.

4.6.3. UV–vis absorption spectroscopy

The steady-state absorption spectra were recorded with a JASCO V-660 spectrophotometer at room temperature and in the spectral range of 200–600 nm, using a 10 mm optical path quartz cuvette.

4.6.4. Differential Scanning Calorimetry (DSC)

The calorimetric experiments were carried out using DSC Q2000 from TA Instruments Inc. (Tzero DSC technology) operating in the Heat Flow T4P option. Measurements were performed under anhydrous high purity nitrogen at a flow rate of 50 mL min^{-1}, with DSC Tzero calibration in the range from −90 °C to 200 °C. PNP dispersions (5 % wt) were dried within the DSC furnace following successive cooling/heating cycles at 10 °C min^{-1} between −70 °C final temperatures gradually increasing from 20 to 100 °C every 10 degrees. Samples with higher crosslinking content were kept at 60 °C during successive periods of 10, 20 and 60 min and posteriorly heated up to 120 °C. Enthalpy (cell constant) and temperature calibration were based on the melting peak of an indium standard (Tm = 156.60 °C) supplied by TA Instruments. Moisturized samples were encapsulated in Tzero (aluminum) hermetic pans with a Tzero hermetic lid with a pinhole to allow water evaporation.

4.6.5. ATR-FTIR spectroscopy

The polymeric films were analyzed by FTIR in a Thermo Nicolet 6700 FTIR spectrometer with a smart miracle ATR accessory (ZnSe crystal). The spectra were measured using an ATR device (Gateway™) and collected after 64 scans for both the background and the sample, with a wave number resolution of 4 cm^{-1}, in the range of 4000–650 cm^{-1}. The measurements were carried out at room temperature with background subtraction.

4.6.6. Mechanical performance evaluation

The mechanical properties of the polymeric films were evaluated with an Instron 3340 and a 50 N load cell, at room temperature. The films were fixed with tensile clamps with an initial preload of 0.01 N, and tested at a constant strain rate of 5 mm min^{-1} until fracture. The elastic tensile modulus (Young's Modulus, E) was obtained from the slope of the linear portion of the stress-strain curve (0–1 % strain). The ultimate tensile strength (σ_f) and the %strain at break (ε_f) were defined, respectively, as the stress and strain values at the point of fracture. The ratio between strength and ductility is obtained by the area under the stress-strain curve and described the toughness (U_T) of the material.

Declaration of competing interest

The authors declare that they have no known competing financial interests or personal relationships that could have appeared to influence the work reported in this paper.

Data availability

Data will be made available on request.

Acknowledgements

The authors acknowledge the financial support of Fundação para a Ciência e a Tecnologia (FCT), projects PTDC/CTM-COM/1581/2021, UIDB/00100/2020, UIDP/00100/2020 and LA/P/0056/2020, and PhD grant SFRH/BD/132486/2017 (T. D. Martins). We thank Prof. Madalena Dionisio for the use of the DSC equipment.

CRediT authorship contribution statement

The work described in the manuscript has not been published previously, is not under consideration for publication elsewhere, its publication is approved by all authors and by the responsible authorities where the work was carried out, and, if accepted, it will not be published elsewhere in the same form, in English or in any other language, including electronically, without the written consent of the copyright-holder.

Appendix A. Supplementary data

Supplementary data to this article can be found online at https://doi.org/10.1016/j.porgcoat.2023.107552.

References

[1] J. Hu, K. Peng, J. Guo, D. Shan, G.B. Kim, Q. Li, E. Gerhard, L. Zhu, W. Tu, W. Lv, J. Yang, M.A. Hickner, ACS Appl. Mater. Interfaces 8 (2016), 17499.
[2] R. Hischier, B. Nowack, F. Gottschalk, I. Hincapie, M. Steinfeldt, C. Som, J. Nanopart. Res. 17 (2015) 1.
[3] J.L. Hall, A. Pérez, E.L. Kynaston, C. Lindsay, J.L. Keddie, Prog. Org. Coat. 163 (2022) 1.
[4] J.Zeno W. Wicks, F.N. Jones, S.P. Pappas, D.A. Wicks, Organic Coatings Science and Technology 3rd ed., 13, Wiley-Interscience, Hoboken, New Jersey, USA, 1985.
[5] J. Yoon, P.A. Lovell, Macromol. Chem. Phys. 209 (2008) 279.
[6] F.N. Jones, M.E. Nichols, S.P. Pappas, Organic Coatings Science and Technology, 4th ed., Wiley, Hoboken, New Jersey, USA, 2017.
[7] M.A. Winnik, P. Pinenq, C. Krüger, J. Zhang, P.V. Yaneff, J. Coatings Technol. 71 (1999) 47.
[8] J.M.G. Martinho, J.P.S. Farinha, in: JCT CoatingsTech 10, 2013, p. 42.
[9] S. Piçarra, C.A.M. Afonso, V.B. Kurteva, A. Fedorov, J.M.G. Martinho, J.P. S. Farinha, J. Colloid Interface Sci. 368 (2012) 21.
[10] X. Ye, J.P.S. Farinha, J.K. Oh, M.A. Winnik, C. Wu, Macromolecules 36 (2003) 8749.
[11] A. Aradian, E. Raphaël, P.G. De Gennes, Macromolecules 33 (2000) 9444.
[12] H. Pham, J.P.S. Farinha, M.A. Winnik, Macromolecules 33 (2000) 5850.
[13] J.P.S. Farinha, O. Vorobyova, M.A. Winnik, Macromolecules 33 (2000) 5863.
[14] A. Aradian, E. Raphaël, P.G. De Gennes, Macromolecules 35 (2002) 4036.
[15] A.R. Mahdavian, Y.G. Jeddi, H. Salehi-Mobarakeh, Adv. Polym. Technol. 30 (2011) 276.
[16] G. Fortunato, V. Marroccoli, F. Corsini, S. Turri, G. Griffini, Prog. Org. Coat. 147 (2020) 1.
[17] M.E. Belowich, J.F. Stoddart, Chem. Soc. Rev. 2012 (2003) 41.
[18] Y. Jin, Q. Wang, P. Taynton, W. Zhang, Am. Chem. Soc. 47 (2014) 1575.
[19] J.P.S. Farinha, S. Piçarra, C. Baleizão, J.M.G. Martinho, in: Industrial Applications for Intelligent Polymers and Coatings, Springer, Gewerbestrasse, Cham, Switzerland, 2016, pp. 619–645.
[20] I.I. Udoh, H. Shi, E.F. Daniel, J. Li, S. Gu, F. Liu, E.H. Han, J. Mater. Sci. Technol. 116 (2022) 224.
[21] L. Fang, J. Chen, Y. Zou, S. Chen, T. Fang, C. Lu, Z. Xu, Macromol. Mater. Eng. 302 (2017) 1.
[22] J. Chen, L. Fang, Z. Xu, C. Lu, Prog. Org. Coat. 101 (2016) 543.
[23] J. Fox, J.J. Wie, B.W. Greenland, S. Burattini, W. Hayes, H.M. Colquhoun, M. E. Mackay, S.J. Rowan, J. Am. Chem. Soc. 134 (2012) 5362.
[24] V.K. Thakur, M.R. Kessler, Polym. (United Kingdom) 69 (2015) 369.
[25] M. Wouters, E. Craenmehr, K. Tempelaars, H. Fischer, N. Stroeks, J. van Zanten, Prog. Org. Coat. 64 (2009) 156.
[26] T. Engel, G. Kickelbick, Polym. Int. 63 (2014) 915.
[27] T. Tamai, P. Pinenq, M.A. Winnik, Macromolecules 32 (1999) 6102.
[28] J. Kötteritzsch, M.D. Hager, U.S. Schubert, Polymer (Guildf). 69 (2015) 321.
[29] S. Parvate, P. Mahanwar, J. Dispers. Sci. Technol. 40 (2019) 519.
[30] J. Machotova, S. Podzimek, P. Kvasnicka, H. Zgoni, J. Snuparek, M. Cerny, Prog. Org. Coat. 92 (2016) 23.
[31] X. Zhang, Y. Liu, H. Huang, Y. Li, H. Chen, J. Appl. Polym. Sci. 2012 (1822) 123.

[32] P. Taynton, K. Yu, R.K. Shoemaker, Y. Jin, H.J. Qi, W. Zhang, Adv. Mater. 26 (2014) 3938.
[33] A. Chao, I. Negulescu, D. Zhang, Macromolecules 49 (2016) 6277.
[34] C.D. Meyer, C.S. Joiner, J.F. Stoddart, Chem. Soc. Rev. 36 (2007) 1705.
[35] M. Ciaccia, S. Di Stefano, Org. Biomol. Chem. 13 (2015) 646.
[36] X. Lei, Y. Jin, H. Sun, W. Zhang, J. Mater. Chem. A 5 (2017) 21140.
[37] P. Chakma, D. Konkolewicz, Angew. Chemie 131 (2019) 9784.
[38] S. Wang, S. Ma, Q. Li, W. Yuan, B. Wang, J. Zhu, Macromolecules 51 (2018) 8001.
[39] S. Slomkowski, J.V. Alemán, R.G. Gilbert, M. Hess, K. Horie, R.G. Jones, P. Kubisa, I. Meisel, W. Mormann, S. Penczek, R.F.T. Stepto, Pure Appl. Chem. 83 (2011) 2229.
[40] I.M. Grabs, G. Schmidt-Naake, Macromol. Symp. 275 (2009) 133.
[41] J.M. Geurts, C.M. Gottgens, M.A.I. Van Graefschepe, R.W.A. Welland, J.J.G. Van Steven Es, A.L. German, J. Appl. Polym. Sci. 80 (2001) 1401.
[42] C. Yan, X. Zhang, Z. Sun, H. Kitano, N. Ise, J. Appl. Polym. Sci. 40 (1990) 89.
[43] J. Zhang, Q. Zou, X. Li, S. Cheng, J. Appl. Polym. Sci. 89 (2003) 2791.
[44] A. Contreras-García, C. Alvarez-lorenzo, A. Concheiro, E. Bucio, Radiat. Phys. Chem. 79 (2010) 615.
[45] W. Chaibi, A. Ziane, Z. Benzehaim, L. Bennabi, K. Guemra, Mater. Sci. Appl. Chem. 33 (2016) 40.
[46] S. Piçarra, A. Fidalgo, A. Fedorov, J.M.G. Martinho, J.P.S. Farinha, Langmuir 30 (2014) 12345.
[47] T.D. Martins, T. Ribeiro, J.P.S. Farinha, Polymers (Basel) 13 (2021) 1.
[48] Y.J. Park, J.H. Kim, Colloids Surfaces A Physicochem. Eng. Asp. 153 (1999) 583.
[49] P. Pinenq, M.A. Winnik 72 (2000).
[50] Y. Miwa, M. Yamada, Y. Shinke, S. Kutsumizu, Polym. Chem. 11 (2020) 6549.
[51] P. Chakma, L.H. Rodrigues Possarle, Z.A. Digby, B. Zhang, J.L. Sparks, D. Konkolewicz, Polym. Chem. 8 (2017) 6534.
[52] L. Guan, H. Xu, D. Huang, J. Polym. Res. 18 (2011) 681.
[53] A. Sidi, J.F. Larché, P.O. Bussière, J.L. Gardette, S. Therias, M. Baba, Phys. Chem. Chem. Phys. 17 (2015) 18751.
[54] B.F. Pierce, G. Tronci, M. Rößle, A.T. Neffe, F. Jung, A. Lendlein, Macromol. Biosci. 12 (2012) 484.
[55] L.M. Polgar, M. Van Duin, A.A. Broekhuis, F. Picchioni, Macromolecules 48 (2015) 7096.
[56] M. Marref, N. Mignard, C. Jegat, M. Taha, M. Belbachir, R. Meghabar, Polym. Int. 62 (2013) 87.